Spatial Resolution Improvement of SSM/I Data with Image Restoration Techniques

Richard Sethmann, Barbara A. Burns, *Member, IEEE,* and Georg C. Heygster

***Abstract*— A space variant image restoration algorithm has been developed with the aim of improving the spatial resolution of SSM/I (Special Sensor Microwave/Imager) passive microwave imagery. Due to the conical scanning of the instrument the relative geometry of the data samples changes over the scan. This change is accounted for here by using a space variant point-spread-function in the restoration algorithm. Application of this algorithm to a scene from the Weddell Sea results in an image with enhanced ice edge and coast definition. As a result ice concentration estimates near the edge agree more closely with higher resolution (optical) data from AVHRR.**

***Index Terms*— Restoration, deconvolution, resolution improvement, SSM/I.**

I. Introduction

THE Special Sensor Microwave/Imager (SSM/I), a satellite passive microwave radiometer, has the advantage over optical and infrared sensors that it can observe large portions of the earth's surface both night and day and through clouds. The SSM/I instrument measures the top-of-atmosphere brightness temperature at 19.35, 37.0, and 85.5 GHz in both the horizontal and vertical polarizations, and at 22.235 GHz channel in the vertical polarization only. In the following text the channels are abbreviated: 19 H, 19 V, etc.

Due to physical limitations on the SSM/I antenna size, the data have relatively poor spatial resolution, with 3 dB footprint sizes of 30 km and larger for the 19, 22, and 37 GHz channels. The spatial resolution of a passive microwave sensor depends both on the antenna size and frequency. Because the SSM/I instrument uses one parabolic reflector for all four frequencies [6], [7], the spatial resolution improves with increasing frequency (see Table I). Most algorithms used to obtain measurements of geophysical parameters, for example the estimation of ice concentration in the polar regions, make use of more than one frequency channel. They therefore require that the area on the surface imaged by different channels be the same. The simplest way to achieve this is to degrade the spatial resolution of all frequencies to that of the lowest resolution channel. However, in order to obtain more accurate measurement of geophysical parameters it would be preferable to improve the resolution of data at low frequencies to that of the higher frequency (higher resolution) data.

Manuscript received July 7, 1993; revised April 8, 1994. This work was supported by the Deutsche Forschungsgemeinschaft (DFG) contracts Ku 709/1-1 and Ku 709/1-2

R. Sethmann is with OHB-System, D-28359 Bremen, Germany.

B. A. Burns and G. C. Heygster are with the Institute of Environmental Physics, University of Bremen/FB1, 28354 Bremen, Germany.

IEEE Log Number 9405534.

TABLE I
SPATIAL RESOLUTION AND SAMPLING INTERVAL OF SSM/I CHANNELS (TAKEN FROM [6])

Channel-Frequency (GHz)	Pol. v/h	Integration-Time (ms)	Resolution (km) along		Sampling Interval (km) along
			track	scan	track/scan
19.35	v/h	7.95	69	43	25
22.235	v	7.95	60	40	25
37.0	v/h	7.95	37	28	25
85.5	v/h	3.89	15	13	12.5

Two types of degradation resulting from the imaging process must be corrected for if resolution is to be improved. The first is the diffraction effect which, as mentioned above, is due to the finite size of the antenna and results in frequency-dependent footprint sizes. Additional blurring occurs in the image data when the sampling interval is such that the footprints overlap. As seen from Table I the amount of overlap in SSM/I data also depends on frequency.

Several recently published studies on resolution enhancement of SSM/I data [1], [2] have used techniques based on a matrix inversion method proposed by Backus and Gilbert [3]. These techniques focus on removing the overlap blur by estimating the contributions to the measured value common to adjacent samples. This clearly requires that the sensor samples are overlapping regions of the two-dimensional distribution of the brightness temperature, and that *a priori* knowledge of the antenna pattern characteristics is available. The result is an estimate of the brightness temperature distribution the sensor would have measured given a prescribed antenna pattern that is narrower than the actual one. The diffraction blur is thereby also effectively corrected.

In this study an image deconvolution technique is used to improve the spatial resolution. As the name implies this approach focuses on correcting for the diffraction blur by removing the low pass filtering effect of the antenna pattern. The goal here is to obtain an estimate of the unsmoothed brightness temperature distribution, ideally as would be measured by an infinitely large antenna. The overlap blur is also reduced in the process. To successfully carry out an image deconvolution requires that the samples are dependent, i.e., that the footprints overlap, as well as information on the antenna pattern. How well the original scene is approximated further depends on the density of the samples (sampling interval). This points up the main differences between the two approaches to resolution improvement: whereas the goal of those based on the Backus–Gilbert method is mainly antenna

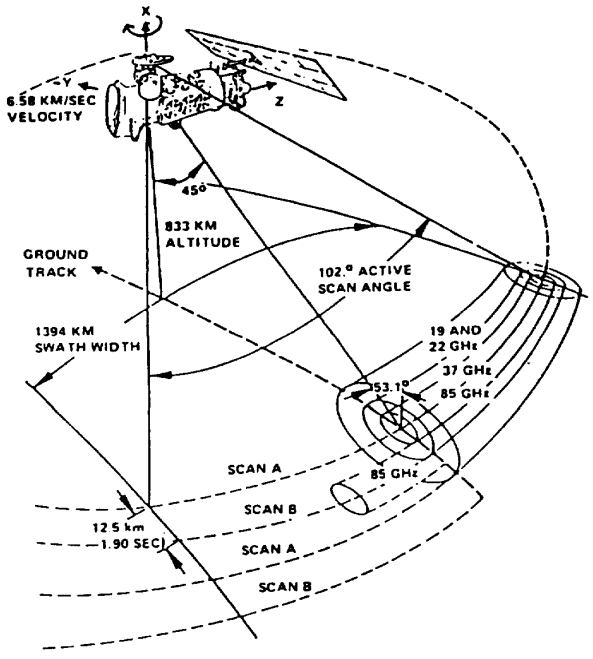

Fig. 1. Scan geometry (taken from [6]).

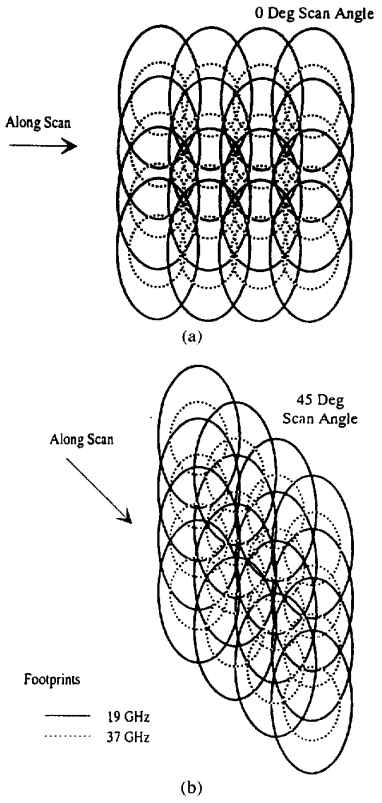

Fig. 2. Relative geometry of SSM/I footprints in a coordinate system on the earth's surface, (a) 0° scan angle, (b) 45° scan angle.

pattern matching, that of the deconvolution techniques is primarily image restoration, i.e., removing the antenna pattern influence.

For the analysis presented here a Wiener deconvolution filter has been applied to SSM/I data in the frequency domain. Due to the conical scanning geometry of the SSM/I the distance between the data points and their relative position to each other changes with position in the scan. Therefore a geometrically adaptive algorithm is used, where the sampling geometry is incorporated in the deconvolution filter itself.

In the next section the SSM/I instrument and the satellite scan geometry are described. Section III discusses the antenna pattern characteristics. Section IV presents the signal model, the deconvolution method and the geometrically adaptive image restoration technique. Section V discusses the results obtained when the restoration technique is applied to SSM/I data from the Antarctic region. Finally, Section IV summarizes our findings.

II. SSM/I Instrument and the Satellite Scan Geometry

The SSM/I is a conical scan instrument rotating continuously about the vertical axis and sampling the earth at scan angles between ±51.2 degrees about the aft direction of the spacecraft (see Fig. 1). It is carried aboard the current Defense Meteorological Satellite Program (DMSP) spacecraft series. The instrument is described in more detail in the SSM/I User's Guide [6] and in [7].

The satellite is in a circular sun-synchronous near-polar orbit at a nominal altitude of 833 km with an inclination of 98.8 degrees and an orbital period of 102.0 minutes. The SSM/I swath width is 1394 km. The lower frequency channels of the instrument (19, 22, and 37 GHz) are sampled every 25 km in both the along scan and along track directions, while the higher frequency channels (85 GHz) are sampled every 12.5 km (see Table I). In each scan 64 discrete radiometric samples are taken at the three lower frequencies and 128 samples are taken at 85 GHz. Scan A in Fig. 1 denotes scans in which all channels are sampled while Scan B denotes scans in which only 85 GHz data are taken.

Due to this conical scanning the relative geometry of the data samples changes over the scan. Fig. 2(a) shows the 3 dB footprints of the 19 GHz (solid ellipses) and 37 GHz (dashed ellipses) channels in the middle of the scan (0° scan angle); the data lie in a nearly rectangular grid. In Fig. 2(b) the data positions near the edge of the scan are shown (45° scan angle). The distance between the samples becomes smaller and the data are no longer in a rectangular grid. This effect is very important for the restoration algorithm (see Section IV). Note that the sampling geometry is symmetrical about the middle of the scan and that the distance between the samples changes more rapidly near the edges of the scan than in the middle.

III. Antenna Pattern Characteristics

The gain functions of the SSM/I antenna (instrument S/N 002 aboard DMSP F8) have been measured in the laboratory before launch, (Hollinger, personal communication). For the 19 GHz channels they were determined at a resolution of

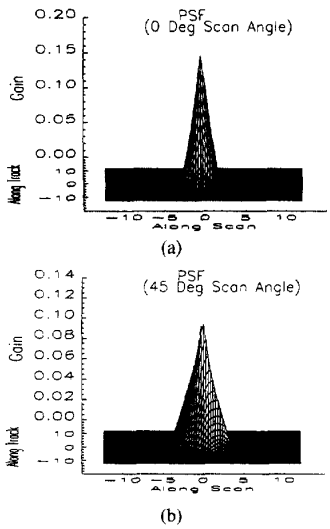

Fig. 3. Point-spread-functions (PSF's) in the same grid as the image data, (a) 0° scan angle, (b) 45° scan angle. The units of the along track and along scan axis indicate number of pixels.

0.1° in elevation angle (displacement from boresight) and at intervals of 45° in azimuth. To produce spatially complete patterns, the gain values at 0.1° intervals in azimuth are estimated using bilinear interpolation. Due to the scan motion of the instrument during observations, the effective antenna beam diameter is larger than the measured antenna pattern width in the along scan direction. The integration time of 7.95 ms used at 19, 22, and 37 GHz translates into an integration region of 1.5°. To obtain the effective antenna pattern a low pass filter of size 1 × 15 therefore has been applied to the measured and interpolated pattern.

The restoration algorithm requires not the antenna pattern but the point-spread-function (PSF). That is the antenna gain distribution in the same grid as the data. Therefore a conversion from the effective antenna pattern to the PSF has to be carried out. In image format the data points (pixels) lie in a rectangular grid regardless of scan angle and therefore the changing relative geometry of the SSM/I footprints has to be incorporated into the PSF. For each sampling point in the scan a PSF is calculated. In the case of the 19 GHz channels 64 PSF's are produced. Fig. 3(a) shows the PSF of the 19 H channel in the middle of the scan (0° scan angle) and Fig. 3(b) the PSF at the right edge (45° scan angle). Comparing this with Fig. 2(b) both data points and PSF are stretched in the diagonal direction.

An important supposition for the restoration is that the image data are dependent samples and that their frequency spectrum has little energy at spatial frequencies higher than half the sampling frequency ($fs/2$ =Nyquist frequency). The sample dependency is assured since the footprint size at 19 GHz is about twice the sampling interval and therefore the measured regions overlap. In general, when the spatial frequency content of a signal to be sampled is unknown, a low pass filter must be applied during measurement such that frequencies higher than the Nyquist frequency are attenuated.

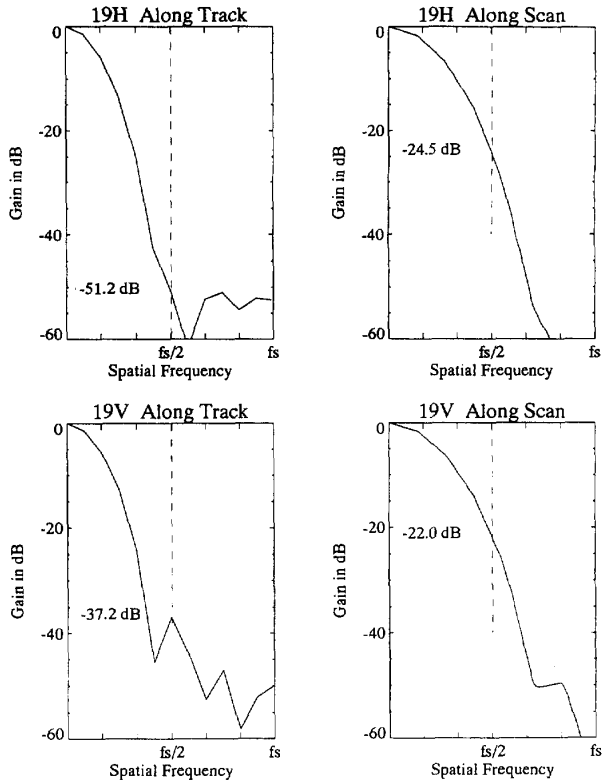

Fig. 4. Profiles of the two-dimensional spectra of the effective antenna pattern (19 GHz channels). The amount of attenuation in dB at half the sampling frequency $fs/2$ is also given.

If not, the spectrum of the measured signal will be aliased. In the case of the SSM/I instrument the effective antenna pattern carries out this low pass filtering for each sample value. But because the antenna pattern is not an ideal low pass filter the two-dimensional frequency spectrum is still but less aliased. Restoration can be carried out, however, if the attenuation by the low pass filter at the Nyquist frequency is large enough so that the contribution from the aliased spectrum is less than the noise level in the signal. An estimate of the necessary attenuation value, calculated from the maximum signal dynamic in the data and the mean noise value of the receiver (see [8]) is about 50 dB.

Figs. 4 and 5 show profiles through the two-dimensional frequency spectra of the effective antenna patterns for the 19 and 37 GHz channels, respectively. The Nyquist frequencies are marked with vertical lines and the corresponding attenuation value is given. With the exception of the 19 H channel the amount of attenuation is less than 50 dB. In the case of the 19 GHz channels the spectra decrease very rapidly in the region of the Nyquist frequencies, and therefore the aliasing of the spectra is restricted to a small region. Due to the narrower antenna patterns of the 37 GHz channels the attenuation at the Nyquist frequency is much less than in the spectra for the 19 GHz channels and the fall-off is less steep. Therefore large portions of these spectra are aliased.

Image restoration generally amplifies the high frequencies of the spectrum and can thereby introduce artifacts when aliasing

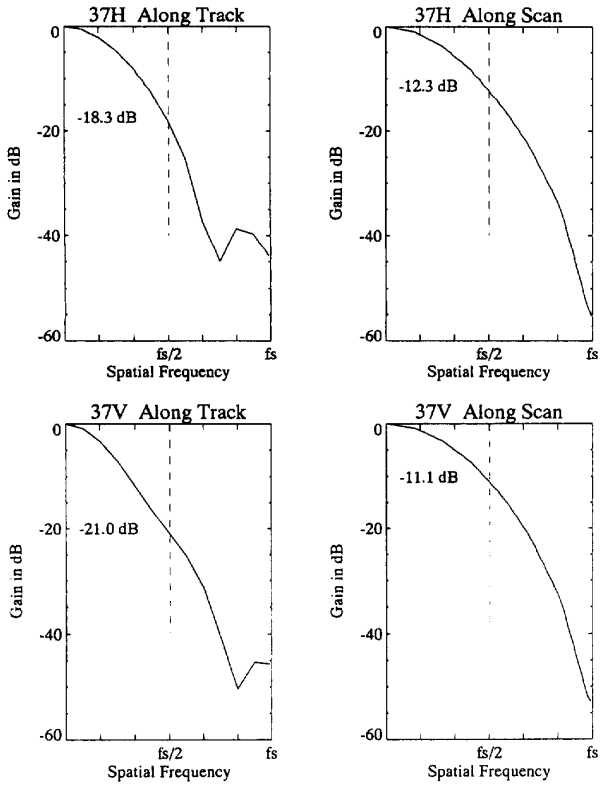

Fig. 5. Profiles of the two-dimensional spectra of the effective antenna pattern (37 GHz channels). The amount of attenuation in dB at half the sampling frequency $fs/2$ is also given.

is severe. For this reason it is advisable, at least for our image restoration approach, to restore only the 19 GHz channels and not those at 37 GHz.

IV. Image Restoration

In this section we describe a signal model for the SSM/I data. It will be shown that the degradation inherent in the imaging process is a linear shift variant one. An image restoration algorithm to improve the spatial resolution is then presented.

Letting p and q be the row and column indexes in the image domain, the at-the-satellite measured data, $d(p,q)$, can be thought of as the sum of the surface brightness temperature distribution, $f(p,q)$, multiplied with the space variant PSF, $h(p,q,i,j)$, plus receiver system noise, $n(p,q)$:

$$d(p,q) = \sum_{i=0}^{M-1}\sum_{j=0}^{N-1} f(i,j)h(p,q,i,j) + n(p,q) \qquad (1)$$

where M, N are the number of rows and columns in the image, respectively. As shown in the previous section the use of a space variant PSF which changes with position in the scan reconciles the conical scan geometry with the placement of data in a rectangular (image) grid.

The aim here is to obtain an estimate, $\hat{f}(p,q)$, of the brightness temperature distribution at the resolution of the pixel spacing. The method described in this paper first simplifies (1) to a convolution of f and h in order to make use of space invariant image restoration techniques. These techniques, including deconvolution in the frequency domain used here, are well established in image restoration literature.

A. Space Invariant Image Restoration

A special case of space variant image restoration is the space invariant one. Equation (1) is then rewritten as the convolution of the brightness temperature distribution, $f(p,q)$, with the space invariant PSF, $h(p,q)$, plus receiver system noise, $n(p,q)$,

$$d(p,q) = \sum_{i=0}^{M-1}\sum_{j=0}^{N-1} f(i,j)h(p-i,q-j) + n(p,q). \qquad (2)$$

The deconvolution is done here in the frequency domain with a linear Wiener filter which minimizes the mean square error between the true image $f(p,q)$ and the deconvolved data $\hat{f}(p,q)$. This filter $Q(k,l,H)$ is composed of an inverse filter $1/H(k,l)$ multiplied by a noise dependent correction term [9], [10]

$$Q(k,l,H) = \frac{1}{H(k,l)}\frac{|H(k,l)|^2}{|H(k,l)|^2 + \Phi_{nn}(k,l)/\Phi_{ff}(k,l)} \qquad (3)$$

where $H(k,l)$ is the two-dimensional Fourier transform of the PSF $h(p,q)$.

The noise dependent term $\Phi_{nn}(k,l)/\Phi_{ff}(k,l)$ is the inverse of the signal-to-noise ratio in the spectrum of the true, but unknown, image, where $\Phi_{nn}(k,l)$ and $\Phi_{ff}(k,l)$ are the power density spectra of the noise $n(p,q)$ and the brightness temperature distribution $f(p,q)$, respectively. The signal-to-noise ratio is unknown but can be estimated from the noise level in the measured data. A frequently adopted approximation is to find an empirical constant value for $\Phi_{nn}(k,l)/\Phi_{ff}(k,l)$ [11]. In this study the empirical value $\Phi_{nn}(k,l)/\Phi_{ff}(k,l) = 0.05$ was used.

B. Space Variant Image Restoration

To adapt the space variant image restoration to the data sampling geometry, two options are available. One is to resample the measured data to a rectangular grid with equidistant sample spacing and use a single Wiener filter in the frequency domain for restoration (space invariant image restoration). This option has been explored in [8] where the resampling was done by a weighted bilinear interpolation of the four nearest neighbors with weights inversely proportional to their distance from the grid cell center. The second option, the method used here, incorporates the data sampling geometry into 64 PSF's, one for each column of the SSM/I data (see Section III). The space variant image restoration can then either be done in the image domain, where the deconvolution will be applied in a local region, or as described in this paper in the frequency domain. The results in [8] show that the first method produces much less edge enhancement than the second method. Additional disadvantages are the calculation time (5 times longer as method two with 64 PSF's) and the loss of information through

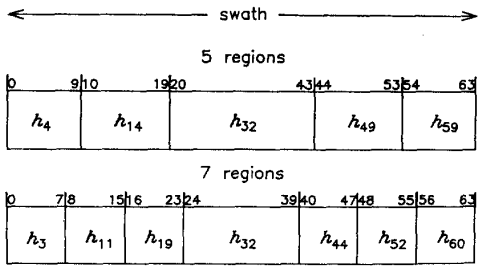

Fig. 6. Division of the scan in 5 and 7 regions.

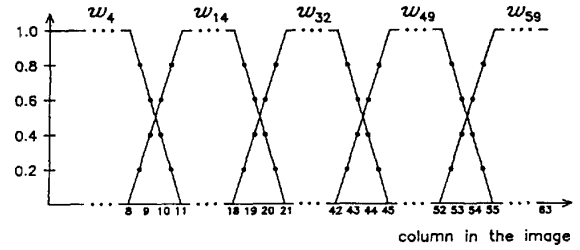

Fig. 7. Choice of the weighting function for the restoration with 5 PSF's.

bilinear interpolation. The latter could probably reduced by using the interpolation method from Poe [5]. In the second method as implemented here 64 deconvolutions are carried out on the entire image, one with each PSF, in the frequency domain with a linear Wiener filter. The desired result, $\hat{f}(p,q)$, is composed by taking one column from each restoration. That is

$$\hat{f}(p,q) = \sum_{i=0}^{N-1} w_i(q)\mathcal{F}^{-1}\{D(k,l)Q(k,l,H_i)\} \qquad (4)$$

where $w_i(q)$ is a weighting function, $D(k,l)$ is the Fourier transform of the image $d(p,q)$, $Q(k,l,H_i)$ the space invariant restoration filter, and H_i the two-dimensional Fourier transform of the PSF h_i. The weighting function chooses from the 64 deconvolution results the one that is right for the qth column in the image. When using 64 PSF's the weighting function is the Kronecker delta function $w_i(q) = \delta_{iq}$. Due to the fact that $d(p,q)$ contains components from neighboring pixels boundary artifacts can be introduced but the neighboring PSF's vary so little that it can be neglected.

To reduce the calculation time it is desirable to carry out the restoration with less than 64 PSF's. In the case of the SSM/I instrument it is possible to restore images with as few as 5 or 7 PSF's, because the PSF's change little from one scan position to the next. Dividing the scan into the 5 or 7 regions shown in Fig. 6 provides a reasonable tradeoff between restoration performance and computation time in the images we have looked at. Due to the conical scan geometry of the SSM/I, the distance between data columns changes more slowly in the middle of the scan compared with the edges (see Fig. 2). Therefore the middle region in Fig. 6 (PSF h_{32}) has more than twice the columns of the other regions. If the scan is divided into 5 regions the PSF h_{49}, calculated for the column 49, is used to restore the region from the column 44 to column 53. If

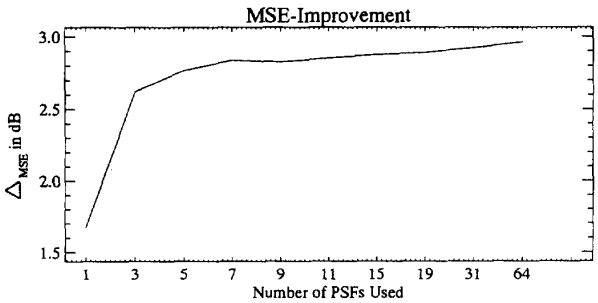

Fig. 8. MSE-improvement versus the number of PSF's used.

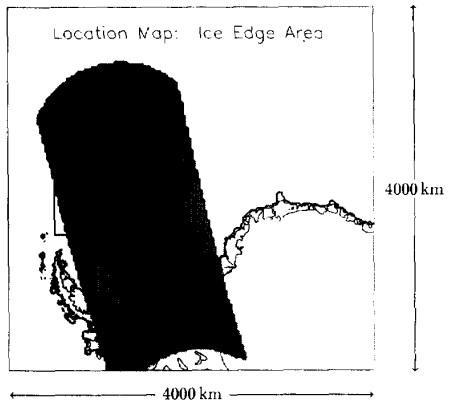

Fig. 9. SSM/I data in the Weddell Sea of 30 September 1989 (polar stereographic projection).

the neighboring PSF's vary greatly (h_{49} and h_{59} for example), artifacts can be introduced into the final result at the boundaries between the partial results. The weighting functions, $w_i(q)$, in (4) are therefore chosen as shown in Fig. 7; the overlapping weighting functions serve to reduce these artifacts, but also result in slight smoothing of the image.

To evaluate the space variant image restoration with less than 64 PSF's a test image has to be blurred according to (1). The used method approximates (1) by first convolving the test image 64 times with different PSF's according to (1). Then the final image is constructed analogously to the restoration result according to (4) by taking the appropriate column from each result and assemble the columns to an entire image. Then Gaussian distributed noise with a mean value of 0 and a variance of 5 grey level values is added. Since the true undistorted image was available, the restoration filter performance could be measured quantitatively using the improvement in MSE (mean square error):

$$\Delta_{\mathrm{MSE}} = 10\log_{10}\left(\frac{\|d-f\|^2}{\|\hat{f}-f\|^2}\right) \qquad (5)$$

where the value of Δ_{MSE} increases with improved resolution.

Space variant restoration of the test image was carried out with 1, 3, 5, 7, 9, 11, 15, 19, 31, and 64 PSF's. In Fig. 8 the Δ_{MSE} improvement versus the number of PSF's used is shown. Between 1 and 3 PSF's the Δ_{MSE} value increases

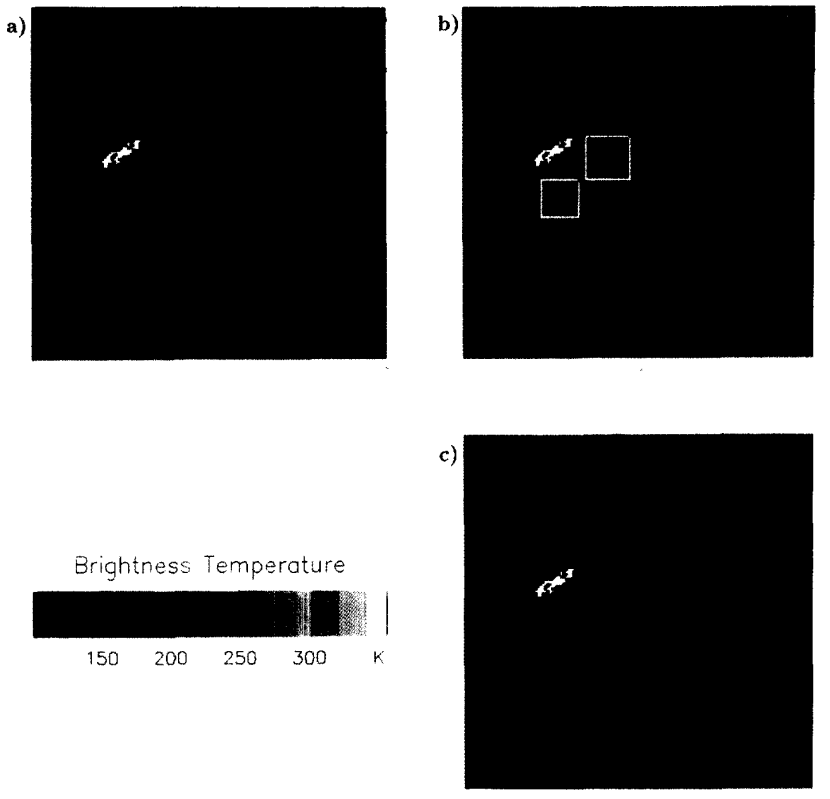

Fig. 10. (a) Measured data from the 19 V channel. (b) Restoration result of (a). (c) Measured data from the 37 V channel.

significantly. Small additional improvement is seen up to 7 PSF's but with the use of more than 7 PSF's the Δ_{MSE} value changes little. Although the best space variant image restoration is achieved with this method by using 64 PSF's, using 5 PSF's produces a good restoration result.

The calculation time on a SUN4/370 (2.7 mega floating point operations per second) for an image size of 128 × 64 pixels is 287 s using 64 PSF's and 25 s using 5 PSF's, almost a factor of 11 reduction. The SSM/I instrument needs 486.4 s to image a scene of size 128 × 64 data points. A real time space variant image restoration with 64 PSF's is therefore feasible, but using 5 PSF's the calculation time is reduced by a factor of 11 and produces similarly good results.

V. Image Restoration Applied to SSM/I Data

The space variant image restoration using 5 PSF's was applied to data from the 19 GHz channels of the SSM/I instrument. The measured data from a single overpass of an Antarctic region (Weddell Sea) in polar stereographic projection are shown in Fig. 9. At the bottom of the SSM/I overpass is the continent, the bright part is sea ice in the Weddell Sea and at the top of the overpass is open water.

The SSM/I restoration results for the 19 GHz channels are compared with data from the higher resolution 37 GHz channel and with data from the Advanced Very High Resolution Radiometer (AVHRR) with a resolution of 1–5 km. This instrument images at visible and infrared wavelengths.

TABLE II
Ice Concentration Comparison with AVHRR

Microwave Data	Bias (% Ice Concentration)	RMS Difference (% Ice Concentration)
measured 19 V & 37 V	9.5	20.3
restored 19 V & measured 37 V	8.0	18.5

The comparison region, indicated with the rectangle in Fig. 9 and shown in more detail in Fig. 10, was chosen because there is an open water/sea ice transition and the coincident AVHRR data are nearly free of cloud. These images show the data projected to a 5-km polar stereographic grid for display purposes only. Black areas are grid points without corresponding data. Image restoration and ice concentration analyses (see Fig. 10) were carried out in the original data format.

Fig. 10(a) shows the measured data from the 19 V channel, Fig. 10(b) the result of the space variant image restoration using 5 PSF's and Fig. 10(c) the 37 V channel. In Fig. 10(b) two regions are marked where an improvement of the spatial resolution is clearly visible. Details are seen which also exist in the 37 V measured data but are not visible in the measured data at 19 V. The reduction in brightness temperature in the middle of the two marked regions in Fig. 10(b) achieved through the restoration also appear in the 37 V channel (Fig. 10(c)).

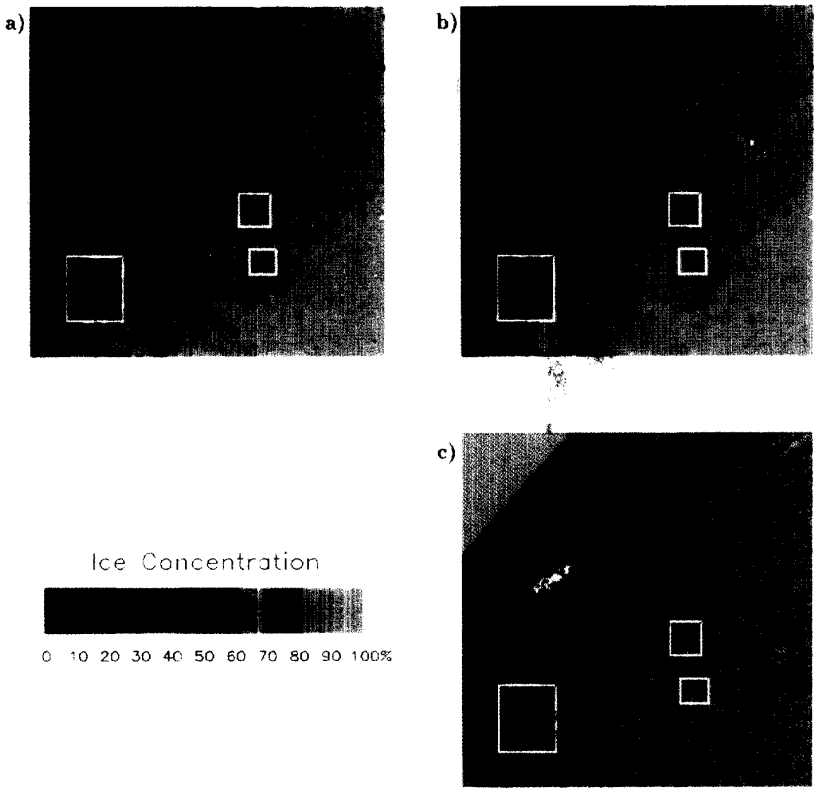

Fig. 11. (a) Ice concentration estimated from measured data. (b) Ice concentration estimated from a combination of measured (37 GHz) and restored (19 GHz) data. (c) AVHRR data.

This qualitative comparison indicates that the resolution of the restored 19 V data more closely matches that of the 37 V channel.

Because the ice edge does not necessarily present a sharply defined boundary, a quantitative estimate of resolution improvement could not be obtained from this scene. However using 19 GHz images of the coast of Australia, [8] was able to estimate the attained resolution by fitting an erf (error function of a Gaussian) to the land-water transition and taking the associated Gaussian half-width as the effective resolution. This analysis showed a resolution improvement of a factor of 1.4, bringing the 19 GHz resolution closer to that at 37 GHz (see Table I).

One application of the improved SSM/I data is in the estimation of the ice concentration. In this study an ice concentration algorithm making use of the 19 V and 37 V channels was applied to data in the original (25 km sample spacing) format. The result from using the measured data is shown in Fig. 11(a); Fig. 11(b) shows the result of using the restored 19 GHz data together with the measured 37 GHz data to estimate ice concentration. The corresponding AVHRR image is shown in Fig. 11(c).

The three rectangles in Fig. 11 mark areas where the agreement between the ice concentration map and the AVHRR image is clearly improved by using the 19 GHz restored data. The two rightmost rectangles correspond to areas with larger regions of open water. This is indicated in Fig. 11(b) by a reduction in the ice concentration, but in Fig. 11(a) the ice concentration is the same as in neighboring areas. The leftmost rectangle contains a transition from sea ice to open water. This water boundary in the restored data agrees better with the AVHRR image than that in Fig. 11(a).

To obtain a quantitative comparison, the AVHRR visible channel data were also analyzed for ice concentration. As seen in Fig. 11(c) the open water portion of the scene is to a large extent cloud covered. This area was masked out (set to an ice concentration of 0%) by applying the 50% ice concentration contour from the passive microwave result to define the ice edge. The ice-covered portion of the scene is only slightly affected by cloud and here ice concentration was calculated using a linear interpolation between ice and water tie points derived from the data [12]. Table II presents the comparison between this result and the ice concentration maps from the measured and combined measured/restored microwave data in terms of bias (microwave-AVHRR) and RMS (root mean square) difference. The magnitude of the difference is not too surprising as the AVHRR data have not been averaged; it therefore includes the natural spatial variability of the ice concentration at scales smaller than the SSM/I footprint. The small effect of cloud cover also contributes to the difference.

But the improvement in the ice concentration estimates with the use of the restored microwave data so clearly seen in the images is borne out in these statistics as well.

VI. Conclusion

This paper has demonstrated the use of an image restoration technique to improve the spatial resolution of the 19 GHz channels of the SSM/I instrument. Because of the SSM/I's conical scanning, the restoration technique must be space variant. This is achieved here by incorporating the sampling geometry into the PSF's. The best restoration result is obtained by using 64 PSF's, one for each scan position. But test data show that use of only 5 PSF's produces a sufficiently good result and reduces the calculation time by a factor of eleven.

The image restoration technique presented can only be applied to the 19 GHz channels because only at this frequency are the data sampled at a sufficiently high rate to satisfy the Nyquist criteria. This is not the case at 37 GHz and therefore restoration of the 37 GHz channels may introduce artifacts in the images due to aliasing in the two-dimensional frequency spectra.

Application of this technique to a sea ice scene showed that features could be resolved in the 19 GHz restoration results which previously were only visible in the higher resolution 37 GHz data. Improvement of the spatial resolution was further evidenced through the use of these restored 19 GHz data to achieve better estimates of ice concentration in the Antarctic region.

Real time application of space variant image restoration is feasible because the time needed to scan a 128× 64 pixel SSM/I scene is a factor of 20 longer than the calculation time required for the restoration. This resolution method would be best integrated into the data processing stream after calibration.

Acknowledgment

The authors wish to thank Prof. Dr. K. F. Künzi, Head of the Institute of Environmental Physics, University of Bremen, for his interest and support, and also Dr. J. P. Hollinger, Naval Research Laboratory, for providing information on the SSM/I instrument.

References

[1] M. R. Farrar and E. A. Smith, "Spatial resolution enhancement of terrestrial features using deconvolved SSM/I microwave brightness temperatures," *IEEE Trans. Geosci. Remote Sensing*, vol. 30, no. 2, pp. 349–355, 1992.

[2] W. D. Robinson, C. Kummerow, and W. S. Olson, "A technique for enhancing and matching the resolution of microwave measurements from the SSM/I instrument," *IEEE Trans. Geosci. Remote Sensing*, vol. 30, no. 3, pp. 419–429, 1992.

[3] G. Backus and F. Gilbert, "Uniqueness in the inversion of inaccurate gross earth data." *Phil. Trans. Roy. Soc. London*, vol. A266, pp. 123–192, 1970.

[4] A. Stogryn, "Estimates of brightness temperatures from scanning radiometer data," *IEEE Trans. Antennas Propagat.*, vol. AP-26, pp. 720–726, 1978.

[5] G. A. Poe, "Optimum interpolation of imaging microwave radiometer data," *IEEE Trans. Geosci. Remote Sensing*, vol. 28, no. 5, pp. 800–810, 1990.

[6] J. P. Hollinger, R. Lo, G. Poe, R. Savage, and J. Peirce, "Special sensor microwave/imager user's guide," Naval Research Laboratory, Washington, DC, 1987.

[7] J. P. Hollinger, J. L. Peirce, and G. A. Poe, "SSM/I instrument evaluation," *IEEE Trans. Geosci. Remote Sensing*, vol. 28, no. 5, pp. 781–790, 1990.

[8] R. Sethmann, *Auflösungsverbesserung von SSM/I Daten durch Bildrestaurationsverfahren*, Düsseldorf: VDI-Verlag, Fortschrittberichte Reihe 10 Informatik/ Kommunikationstechnik Nr. 241, Dissertation Universität Bremen 1993.

[9] R. Sethmann, G. Heygster, and B. A. Burns, "Image deconvolution techniques for reconstruction of SSM/I data," in *Proc. IGARSS '91*, Helsinki, Finland, IEEE Catalog No. 91CH2971-0, 1991, pp. 2377–2380.

[10] F. M. Wahl, *Digital Image Signal Processing*. Boston, MA: Artech House, 1987.

[11] A. Rosenfeld and A. C. Kak, *Digital Picture Processing*. New York: Academic, 1976.

[12] B. A. Burns, M. Schmidt-Gröttrup, and T. Viehoff, "Methods for digital analysis of AVHRR sea ice images," *IEEE Trans. Geosci. Remote Sensing*, vol. 30, no. 3, pp. 589–602, Mar. 1992.

Richard Sethmann was born in Volkmarst, Germany, on March 1, 1961. He received the B.Sc. degree in electrical engineering from the Hochschule Bremen in 1986 and the M.Sc. degree from the University of Bremen in 1989 in information theory and digital image processing. He received the Ph.D. degree in physics in 1992 specializing in remote sensing research concerning the resolution improvement of passive microwave data with image restoration techniques.

Since 1993 he has been with the space company OHB-System (Orbital and Hydrotechnology Bremen), where he has worked mainly in the data processing field.

Barbara A. Burns (A'85–M'85) received the B.Sc. degree in physics and mathematics from the University of Wisconsin-Eau Claire in 1975, and the Ph.D. degree in astronomy from Cornell University, Ithaca, NY, in 1982.

From 1981 to 1988 she was with the Radar Science Laboratory of the Environmental Research Institute of Michigan, where she worked primarily on development of algorithms for measurement of sea ice properties with synthetic aperture radar. Between 1987 and 1990 she held a position as Visiting Scientist at the Alfred-Wegener-Institut für Polar- und Meeresforschung, Bremerhaven, Germany. She is currently at the Institute of Environmental Physics of the University of Bremen, Germany, where her research deals with using satellite passive microwave data to measure rainfall rate over land and ocean, and to discriminate ice-water boundaries in polar regions.

Georg C. Heygster was born in 1951 in Braunschweig, Germany. He received the degree of Diplomphysiker in 1976 in the field of solid state physics and the Dr. rer. nat. degree in 1979 in the field of processing medical images, both from the University of Göttingen.

From 1979 to 1988 he worked as a consultant in the computer center of the University of Bremen. Since 1988 he has been the head of the Physical Satellite Image Analysis group of the Institute of Environmental Physics (former Institute of Remote Sensing) of the University of Bremen. His research activities have been in the fields of passive microwave remote sensing, especially of the cryosphere and resolution improvement of passive microwave data.